

# Live-Cell Characterization and Analysis of a Clinical Isolate of Bovine Respiratory Syncytial Virus, Using Molecular Beacons

Philip Santangelo,<sup>1</sup> Nitin Nitin,<sup>1</sup> Leslie LaConte,<sup>1</sup> Amelia Woolums,<sup>2</sup> and Gang Bao<sup>1\*</sup>

*Department of Biomedical Engineering, Georgia Institute of Technology and Emory University, Atlanta, Georgia 30332,<sup>1</sup> and Department of Large Animal Medicine, College of Veterinary Medicine, University of Georgia, Athens, Georgia 30602<sup>2</sup>*

Received 8 June 2005/Accepted 18 October 2005

**Understanding viral pathogenesis is critical for prevention of outbreaks, development of antiviral drugs, and biodefense. Here, we utilize molecular beacons to directly detect the viral genome and characterize a clinical isolate of bovine respiratory syncytial virus (bRSV) in living cells. Molecular beacons are dual-labeled, hairpin oligonucleotide probes with a reporter fluorophore at one end and a quencher at the other; they are designed to fluoresce only when hybridizing to a complementary target. By imaging the fluorescence signal of molecular beacons, the spread of bRSV was monitored for 7 days with a signal-to-noise ratio of 50 to 200, and the measured time course of infection was quantified with a mathematical model for viral growth. We found that molecular beacon signal could be detected in single living cells infected with a viral titer of  $2 \times 10^{3.6}$  50% tissue culture infective doses/ml diluted 1,000 fold, demonstrating high detection sensitivity. Low background in uninfected cells and simultaneous staining of fixed cells with molecular beacons and antibodies showed high detection specificity. Furthermore, using confocal microscopy to image the viral genome in live, infected cells, we observed a connected, highly three-dimensional, amorphous inclusion body structure not seen in fixed cells. Taken together, the use of molecular beacons for active virus imaging provides a powerful tool for rapid viral infection detection, the characterization of RNA viruses, and the design of new antiviral drugs.**

Rapid detection of viral infections and understanding viral pathogenesis are crucial for the prevention of an infectious disease outbreak, development of antiviral drugs, and biodefense. One of the predominant routes for viruses to enter a host is via the respiratory tract (22). Even though the respiratory mucosal environment and associated cells have many methods of preventing viral entry, many viruses, such as influenza virus, severe acquired respiratory syndrome-associated coronavirus, parainfluenza virus, and respiratory syncytial virus (RSV), find ways of thwarting the body's many defenses and taking up residence within the cells of the respiratory tract (16). Some viruses, such as influenza virus and RSV, cause local respiratory infections, while others, such as varicella-zoster virus, mumps virus, and measles virus (22), use the respiratory tract as an entryway to other parts of the body. There is a definite need for rapid, simple, sensitive, and specific tests for common viruses and for emerging infectious agents, such as severe acquired respiratory syndrome-associated coronavirus, highly virulent viruses such as influenza H5N1 (avian flu) (12), and possible bioterror agents such as variola virus (which causes smallpox).

In addition to detecting viruses, there is a strong need to develop tools to study the pathogenesis of viruses and their response to antiviral agents. In recent years, new classes of antiviral molecules with potential clinical applications have been developed, including small interfering RNA (2, 41) and fusion inhibitors such as enfuvirtide for human immunodeficiency virus type 1 and a nonpeptide small molecule for RSV

(6). New methods that allow the rapid evaluation of the direct effect of antiviral drugs in live cells will be extremely helpful in expediting their development.

Existing methods for studying viral replication and infection include viral isolation and culture, electron microscopy, antibody-based assays (direct fluorescent antibody and enzyme-linked immunosorbent assay), and nucleic acid-based assays (real-time reverse transcription-PCR [RT-PCR] and fixed-cell in situ hybridization) (26). Viral isolation and culture are still the "gold standard" but are rapidly being replaced by molecular methods such as enzyme-linked immunosorbent assay and RT-PCR (16). Both of these molecular methods are very sensitive and specific but labor intensive; neither can be used with live cells. Further, these methods lack the ability to localize and track target nucleic acids in infected cells. Consequently, it is not possible to gain insight into the molecular mechanisms involved in replication, intracellular organization, and cell-to-cell transfer of viruses by RT-PCR or other in vitro methods.

RNA molecules in a live cell can be imaged using tagged full-length RNAs (15, 18, 19) and green fluorescent protein-tagged RNA-binding proteins (5, 11, 13). For example, after their isolation, fluorescently labeled RNAs and ribonucleoproteins (RNPs) have been introduced into living cells by microinjection to monitor the localization of specific RNAs or to track specific viral RNPs (19). The transport and localization of both cytoplasmic and nuclear RNAs have been studied by using an RNA-binding protein, MS2 (13, 35). Although these novel approaches can provide a powerful tool for studying RNA biology, it is difficult to apply these methods to study viral pathogenesis in living cells. Specifically, the process of isolating viral RNPs and the conjugation of a large number of dye molecules to the viral RNA or the associated proteins may significantly affect the function and dynamics of target RNA.

\* Corresponding author. Mailing address: Department of Biomedical Engineering, Georgia Institute of Technology and Emory University, 313 Ferst Dr., Suite 2115, Atlanta, GA 30332. Phone: (404) 385-0373. Fax: (404) 894-4243. E-mail: gang.bao@bme.gatech.edu.

Further, for a clinically isolated virus, as is the case in this study, it is difficult to engineer the MS2-binding sites into the viral genome, thus precluding the application of this method.

In this paper, we describe the rapid detection and analysis of RNA viruses in live cells with molecular beacons (MBs). MBs are dual-labeled oligonucleotide probes with a reporter fluorophore at one end and a quencher at the other. They are designed to form a stem-loop hairpin structure so that fluorescence occurs only when the probe hybridizes to a complementary target, resulting in a high signal-to-background ratio. Although MBs have been used in PCR assays for viral infection detection (1) and in very limited studies of living-cell gene detection (4, 28, 30, 32, 34, 36, 38), their potential application in rapid detection and analysis of virus in living cells has not been demonstrated.

For this study we chose RSV, one of the most common causes of infantile hospitalization in the developed world (8). RSV also accounts for considerable morbidity and mortality in the elderly, the immunocompromised, and those with chronic diseases or in long-term care facilities (17). Using molecular beacons designed to target several repeated sequences of the gene end-intergenic gene start signal within the human RSV (hRSV) and bovine RSV (bRSV) genome, we are able to provide new and important information regarding viral structure and dynamics in single living cells. This is, to our knowledge, the first report of the use of molecular beacons to study the spreading of a viral infection and to observe the structure of inclusion bodies in live cells due to a clinically relevant virus. We also applied a viral growth model to quantitatively evaluate virus growth and spreading.

## MATERIALS AND METHODS

**Cells and viruses.** Primary bovine turbinate cells (American Bioresearch, Tennessee) were grown in Dulbecco's modified essential medium (Sigma Aldrich) with 5% horse serum and 5% goat serum with 100 U of penicillin/ml and 100 mg of streptomycin/ml. The virus used is a clinical isolate of bRSV, CA-1, obtained from Laural Gershwin's laboratory at the University of California, Davis, from a fatal case of bRSV infection of a cow in 1986. Cells were infected with a multiplicity of infection of 0.2; virus was identified by direct fluorescent antibody staining. All cells were infected at a confluence of approximately 50 to 70% by removing the medium and washing the cells in phosphate-buffered saline (PBS) with  $\text{Ca}^{2+}$  and  $\text{Mg}^{2+}$ , and then adding virus directly to the cells for 30 min at 37°C. After a 30-min incubation, regular medium was added.

**Molecular beacon synthesis and characteristics.** To enhance the sensitivity of the measurements, the MB probe used for this study, 5'-Cy3-CGACGAAAAATGGGGCAAATACGTCG-BHQ-2-3' (the stem is underlined and the hybridization domain is in italics; BHQ is a designation for black hole quencher) was designed such that it targets several repeated sequences that occur within the critical gene end-intergenic gene start signals of the hRSV and bRSV genome. The MB was synthesized by Biosource International (Camarillo, CA) and was tested first in solution by using a short synthetic oligonucleotide target, 5'-TATTTGCCCATTTTT-3'. The solution study of probe target hybridization was carried out in a 1× PBS buffer without calcium and magnesium using a Safire fluorescent microplate fluorometer (Tecan, Zurich, Switzerland), with 545-nm excitation and 560- to 620-nm emission detection. Concentrations of 200 nM molecular beacon and 400 nM target were used in a total volume of 50  $\mu\text{l}$ . In addition, a control beacon with the sequence 5'-Cy3-CGACGAAAAATAAACAAATACGTCG-BHQ-2-3 was designed with mismatches (four adenines replaced the four guanines) in the critical G-repeat region of the MB. This control MB, when checked in the BLAST search, showed no exact match except in monocots and bacteria. This MB was used to verify the specificity of the MB designed to target the bRSV genome in infected cells.

**Molecular beacon delivery.** MBs were delivered into infected and uninfected live primary bovine turbinate cells on days 1, 3, 5, and 7 postinfection (p.i.) using a reversible permeabilization method with streptolysin O (SLO), which was

shown to be a rapid, efficient, less-damaging, and more versatile (in terms of cell type) method than conventional transfection (9, 34). It has also been shown that the SLO-based method can be used with any cell type (primary cells or cultured cell lines) that contains cholesterol in its plasma membrane that facilitates SLO attachment and membrane pore formation (9, 34). The delivery efficiency, therefore, may be cell-type dependent. Cells grown in normal medium were first washed with serum-free medium and then incubated with a mixture of 0.2 U of SLO/ml and 2  $\mu\text{M}$  MB in an appropriate amount of serum-free medium for 10 min at 37°C. The SLO-MB-serum-free medium was then removed and replaced by fresh normal medium. The cells were imaged either by epifluorescence or confocal microscopy 20 min after incubation. We found that when SLO was used, MBs were delivered into bovine turbinate cells with nearly 100% efficiency.

**RNA staining of live cells and simultaneous staining of fixed cells.** To show that the inclusion bodies formed by bRSV in living cells are actually composed of RNA, infected and uninfected live cells were stained with SytoRNAselect at a concentration of 500 nM in regular medium per the protocol provided by Molecular Probes. After a 30-min incubation, the cells were washed with PBS and imaged in regular medium by epifluorescence microscopy with a Chroma filter set (41001) for fluorescein.

To confirm infection of bRSV-inoculated cells (in addition to the observation of cytopathic effect), cells were simultaneously stained with both MBs for the viral genomic RNA of bRSV and with a monoclonal antibody (MAb) for the bRSV F protein. The MAb, designated 8G12, was provided by C. Kelling at the University of Nebraska; its specificity and use in direct fluorescent assays have been reported previously (21). Infected and uninfected live cells were stained with the bRSV-specific molecular beacon as discussed above. After MB staining, the live cells were fixed with ice-cold 4% paraformaldehyde in PBS for 10 min. They were then washed twice with 1× PBS for 5 min and incubated with a 1:100 dilution of Alexa 488-labeled (Molecular Probes) monoclonal 8G12 in PBS for 30 min at 37°C. After being washed twice with 1× PBS for 5 min, these cells were imaged with an epifluorescence microscope.

**Fluorescence microscopy imaging.** Fluorescence imaging of bRSV spreading and the results of serial dilution, RNA staining, and simultaneous staining were performed using a Zeiss Axiovert 100 TV epifluorescence microscope coupled to a Cooke Sencim SVGA cooled charge-coupled device camera. For inclusion body structure studies of live and fixed cells, the Zeiss LSM Meta 100 confocal microscope was used. The pinhole for confocal microscopy was set such that each image was 0.5  $\mu\text{m}$  thick, with 0.5  $\mu\text{m}$  between images. For molecular beacon assays, excitation and emission detection experiments were performed using 545- and 570-nm filters, respectively. For imaging Alexa 488, fluorescein optics were used. An exposure time of 0.1 s was used for all wide-field imaging assays. Signal-to-noise ratios were calculated based on the maximum signal intensity within an inclusion body divided by the average background pixel value from a portion of the field of view not containing any cell. Images were false colored using the "black body" color map provided by Adobe Photoshop or 256 shades of red. To compare experimental data with the viral growth model, ImageJ, version 1.33u (National Institutes of Health), was used to count the number of uninfected cells per image and quantify the rate of uninfected cell growth, as well as the number of infected cells per image. Averages and standard deviations were calculated using Microsoft Excel.

**Solver for coupled set of differential equations.** The Maple (version 9.5) ordinary differential equation (ODE) solver, dsolve, was used to solve the nonlinear, coupled set of differential equations that describe viral growth dynamics. Inputs to the solver were three nonlinear, differential equations and their initial conditions.

## RESULTS AND DISCUSSION

**bRSV as a model system.** In this study, bRSV was used as a model for hRSV, due to its genetic similarity to hRSV (23, 27) and its pathological and epidemiological similarities to RSV-induced disease in humans. It may also be used in future evaluation of the MB-based method for in vivo detection of RNA viruses (39), which has the potential to expedite treatment or vaccine development. *Bovine respiratory syncytial virus*, a member of the family *Paramyxoviridae*, is an enveloped virus, containing an unsegmented, negative-stranded RNA genome of approximately 15,000 nucleotides (7). The genome encodes 10 viral proteins that are translated from individual messenger RNAs. Viral titers used in this study for the progression of

virus, serial dilution experiments, and inclusion body structure experiments were evaluated to be approximately  $2 \times 10^{3.6}$  50% tissue culture infective doses (TCID<sub>50</sub>)/ml, which is approximately the same ( $10^{3.6}$  versus  $10^4$ ) as that originally isolated by Loral Gershwin's laboratory. These titers have been used by Amelia Woolums' laboratory at the University of Georgia in their animal studies of bRSV infections in cattle (39).

**Molecular beacon design and solution study.** The MB designed for this study targets a gene end-intergenic gene start sequence, 3'-UUU UUA CCC CGU UUA U-5', which has three exact repeats (at the 3' leader-NS1 gene and between, respectively, the NS1-NS2 and N-P genes) and six almost-exact repeats with various numbers of nucleotide mismatches (10, 20). Similar intergenic repeats are common in other RNA viruses (37). Successfully used in antisense and small interfering RNA experiments (20, 33, 40), this site was considered the most accessible and therefore a prime site for oligonucleotide binding and probe targeting. Targeting the repeated sequences allows the binding of three to nine molecular beacons to each viral genome, providing signal amplification and significantly increasing the signal-to-noise ratio. Since the target is concentrated in viral factories (inclusion bodies), the signal is further enhanced.

The bRSV-targeting molecular beacon was tested first in solution with a short synthetic DNA target to obtain the signal-to-noise ratio of the beacon. The maximum signal-to-noise for this beacon in solution was approximately 30. Because of the signal amplification due to multiple hybridization sites per viral RNA and the accumulation of viral RNA in inclusion bodies, single, unpaired MBs were used in this study instead of the dual-beacon approach (34).

**Molecular beacon delivery.** In contrast to most living-cell gene detection assays, we used a reversible permeabilization delivery method in this study with SLO, which was shown to be a rapid, efficient, less-damaging, and more versatile method than conventional transfection (34) and microinjection. Most attempts in detecting specific RNAs in living cells used microinjection of fluorescently labeled linear or hairpin oligonucleotide probes, resulting in sequestration of the probes in the nucleus and prevention of measurements of cytoplasmic RNA (29, 32, 36). Further, microinjection is an inefficient method for viral pathogenesis studies, since the infected cells are not known a priori, and therefore a whole population of cells, infected and uninfected alike, would need to be microinjected, which is slow and labor intensive. The SLO-based probe delivery method can also be used to deliver both MBs targeting viral genome and probes targeting viral proteins.

**Progression of viral infection in live cells.** To study the dynamics of viral infection, bovine turbinate cells were plated in four-well, chambered coverslips and grown to 50 to 70% confluence before being inoculated with bRSV per Materials and Methods. Molecular beacons targeting the bRSV genome were delivered into both infected and uninfected live cells with SLO on days 1, 3, 5, and 7 postinfection; the resulting fluorescence signal in these cells was observed on these days to follow the progression of the infection. We found that the progression of the infection in live cells could be characterized quickly (<30 min) using MBs. Shown in Fig. 1 are probe-target hybridization-induced fluorescence signals in infected and uninfected cells (as a negative control), following the progression of

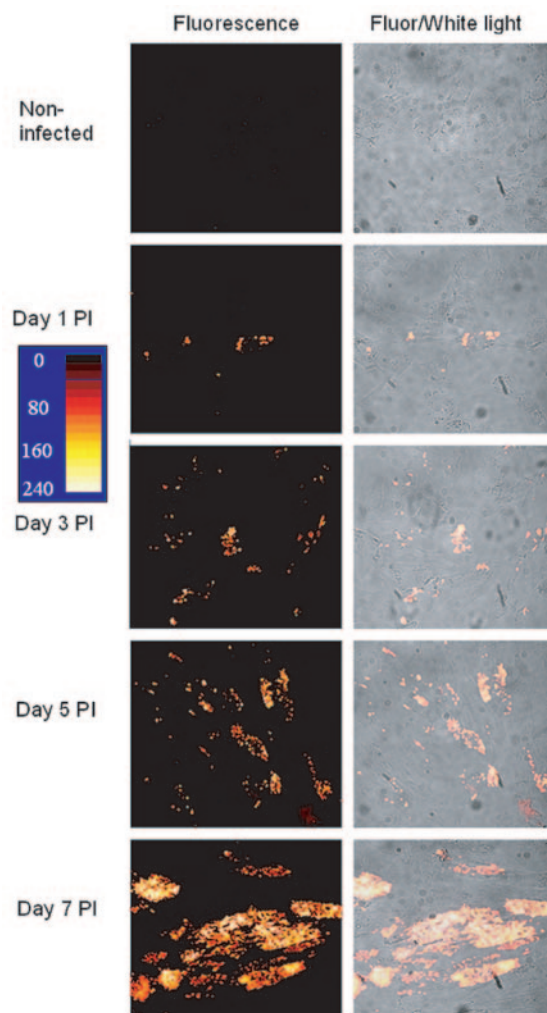


FIG. 1. Live-cell fluorescence imaging of bRSV viral genome following the progression of infection for 7 days p.i. The left column contains fluorescence images of infected cells and the right column contains overlay images of the fluorescence and white-light observations of cells.

bRSV infection for 7 days. It is clear that even on day 1 postinfection, the infected cells were easily distinguished from the uninfected cells and the localized inclusion bodies could be observed with signal-to-noise ratios ranging from 50 to >200. The fluorescence signal of MBs was predominately found in inclusion bodies, which were not always visible by white-light phase-contrast microscopy. The very low background signal in uninfected cells as shown in Fig. 1 suggests that the MB-based viral detection method has a high specificity. In addition, the average ratio of background fluorescence within the cells to regions without cells or within the cell nucleus (where no MBs were internalized) was approximately 1.5 for 5 to 7 days. This was most likely due to the fact that in our experiments cells became confluent within the first 24 h postinfection, resulting in a low enzyme activity level in the cytoplasm of nondividing cells.

The progressively increased number of infected cells during the 7-day period as indicated by the fluorescence images in Fig.

1 of viral genome at days 1, 3, 5, and 7 p.i. clearly demonstrated the ability of MBs to monitor and quantify in real time the spreading of viral infection, which has significant implications for studies of the dynamics and kinetics of viral replication and cell-cell transmission of RNA viruses in a cell population.

**Quantitative studies of viral infection spreading.** To quantify the spreading of bRSV infection in living cells, we employed the software ImageJ (version 1.33u; National Institutes of Health) to count the number of infected cells per image using fluorescence images similar to that shown in Fig. 1. The growth rate of uninfected cells was also obtained. Following Bonhoeffer et al. (3), we adopted a viral growth model in which the basics of viral dynamics were captured with three variables: the number of uninfected cells,  $x$ ; the number of infected cells,  $y$ ; and the number of free virus particles,  $z$ . The differential equations describing the viral growth and spreading in cells are as follows:

$$\frac{dx}{dt} = \lambda - \beta xz \quad (1)$$

$$\frac{dy}{dt} = \beta xz \quad (2)$$

$$\frac{dz}{dt} = \alpha y - \gamma z \quad (3)$$

where  $\lambda$  is the rate of growth for uninfected cells,  $\beta$  is a rate constant representing the rate at which normal cells become infected by one free viral particle,  $\alpha$  is the rate constant for virus particles budding from infected cells, and  $\gamma$  is the rate constant representing the death of viral particles. Since there was very little cell death during our experiments, the rates at which infected and uninfected cells died were assumed to be zero. This set of nonlinear first-order ODEs were solved numerically using dsolve, the Maple (version 9.5) ODE solver, to give the number of infected cells as a function of time (days), with the following initial conditions:  $x(0) = 50$  (the initial number of uninfected cells, averaged over 10 experimental observations),  $y(0) = 0$ , and  $z(0) = 0.17$  (the average initial number of virus particles per 50 cells), estimated from the experimental conditions and multiplicity of infection value. The rate of growth of uninfected cells was taken to be  $\lambda = 3.0$  cells/day, based on the average growth rate from 10 experimental observations. The other rate constants were chosen to be  $\beta = 2.3$  (1/virus particle day),  $\alpha = 1.7$  (virus particle/cell day), and  $\gamma = 1.0$  (1/day) based on the experimental data of viral growth for days 1, 3, and 5 p.i. Specifically, a cell was deemed infected if there were one or more fluorescent inclusion bodies inside the cell and the error bars for the experimental data shown in Fig. 2 were calculated from 10 experimental observations at each condition.

Shown in Fig. 2 is the model prediction for viral growth over a 13-day period, along with the experimental results for days 1 to 7 postinfection. It is seen from Fig. 2 that the model could predict the viral spreading for day 7 quite well based on experimental data from days 1, 3, and 5. In addition, it predicts a significant decrease in the rate at which cells are infected after day 9, which has been observed in cell culture (data not shown). Further, the rate constants  $\alpha$ ,  $\beta$ ,  $\gamma$ , and  $\lambda$  can be used

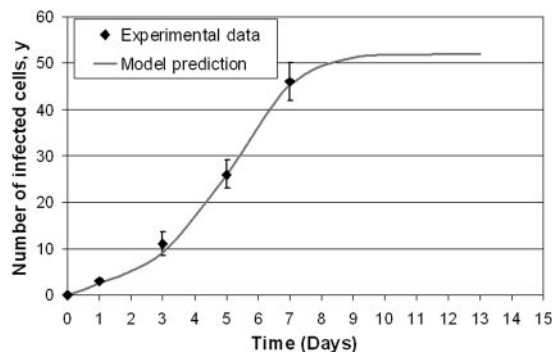


FIG. 2. Comparison of model prediction and experimental data for spreading of viral infection. The number of infected cells ( $y$ ) is plotted as a function of time (days), showing the progression of infection over a 13-day period. The parameters for the model were determined either independently ( $\lambda$ ) or from the measurements of days 1, 3, and 5 postinfection ( $\alpha$ ,  $\beta$ , and  $\gamma$ ). Comparison between prediction and experimental data for the number of infected cells at day 7 postinfection showed good agreement, indicating the predictive capability of the model. Note that the number of infected cells reached a plateau around day 9 postinfection.

as a set of parameters to compare quantitatively the growth behavior of different viruses.

**Detection sensitivity.** To show the detection sensitivity of the MB-based method, serial dilutions of virus stock ( $10^0$ ,  $10^{-1}$ ,  $10^{-2}$ , and  $10^{-3}$ ) were used to infect bovine turbinate cells at 50% confluence. After 12 days p.i., live-cell MB assays were performed, and the resulting fluorescence in infected cells was imaged using epifluorescence microscopy. The results of serial dilutions of virus stock are displayed in Fig. 3A to D. It can be seen from Fig. 3 that even when a virus of titer  $2 \times 10^{3.6}$  TCID<sub>50</sub>/ml is diluted 1,000 fold (Fig. 3D), evidence of virus activity could still be observed with standard imaging equip-

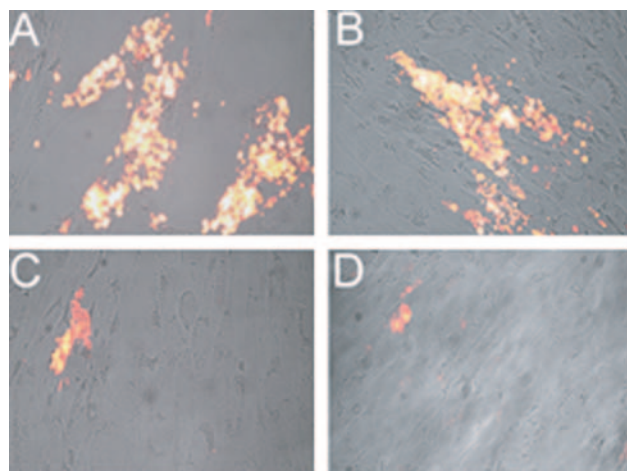


FIG. 3. Detection sensitivity studies utilizing serial dilutions of virus stock. Virus with a titer of  $2 \times 10^{3.6}$  TCID<sub>50</sub>/ml was diluted to dilutions of  $10^0$  (A),  $10^{-1}$  (B),  $10^{-2}$  (C), and  $10^{-3}$  (D) and was used to infect four-well plates of bovine turbinate cells at 50% confluence. They were imaged 12 days after infection, at which time there were no more signs of increasing cytopathic effect. Note that viral infection could be detected in single cells even at a 1,000-fold dilution of virus stock.

ment. Clearly, single infected cells could be readily identified. It is possible that with a more sensitive camera or the use of a confocal microscope with photon-counting capability, single-virus RNA detection sensitivity may be achieved with a wild-type virus.

**Structure of inclusion bodies in live and fixed cells.** The presence of cytoplasmic inclusion bodies in RSV-infected cells was first observed by electron microscopy (31). Inclusion bodies, made of aggregated nucleocapsids, have also been observed in the cytoplasm of cells infected with other paramyxoviruses. Typically, to observe the structure of the inclusion bodies, the infected cells need to be fixed with cold methanol-acetone or formaldehyde-glutaraldehyde and stained with monoclonal antibodies against the major viral structural proteins (14). Antibody staining of RSV in fixed cells reveals circular aggregates of virus, with some amorphous material surrounding them (14). Inclusion bodies were always found in the cytoplasm. However, no live-cell imaging of inclusion bodies has been reported to date.

An important feature of the MB-based imaging approach is the ability to determine the location of the viral genome within the cell and to allow observation of the structures formed by the viral RNP while the cell is still alive and the virus is active. To visualize virus structure and organization in host cells, we performed live-cell MB assays of cells that were 7 days p.i. and imaged them with a scanning confocal microscope, which enabled the imaging of the three-dimensional structure of the inclusion bodies in living cells. The results from a typical infected cell are displayed in Fig. 4A. Starting from the top left corner of the figure, each image represents a 0.5- $\mu\text{m}$ -thick slice of the cell; these images were taken from the bottom of the cell (closest to the coverslip), with a 0.5- $\mu\text{m}$  gap between them. We found that inclusion bodies in live cells had a complex morphology; many of them were elliptical, twisted, and in very close contact, with an extended structure throughout the thickness of the cell (approximately 6.5- $\mu\text{m}$  thick; not all of the slices are shown). When infected cells containing MB-stained inclusion bodies were fixed in ice-cold, 4% paraformaldehyde for 10 min, very consistent characteristic changes in the inclusion body structure were observed with the same confocal setup, as shown in Fig. 4B. In all of the cells fixed, the inclusion bodies were uniformly spherical in morphology and seemed to be less connected than those imaged in live cells. Although fluorescence in situ hybridization can detect mRNAs in fixed cells with high sensitivity (24, 25), it appears that live-cell imaging of inclusion body structure offers significant advantage over a fluorescence in situ hybridization method.

The cytoplasmic inclusion bodies are aggregates of viral RNPs vital to the production of viral genome and proteins. Understanding the structural details of inclusion bodies will help gain insight into the mechanisms by which the inclusion body is formed and how it can be disrupted. Therefore, the ability of the MB-based method to visualize the detailed three-dimensional organization of the viral machinery in live cells promises to open new opportunities for studying the dynamics of viral replication and packaging inside an infected cell, the association of the viral machinery with subcellular structures such as cell cytoskeleton, and the development of antiviral drugs.

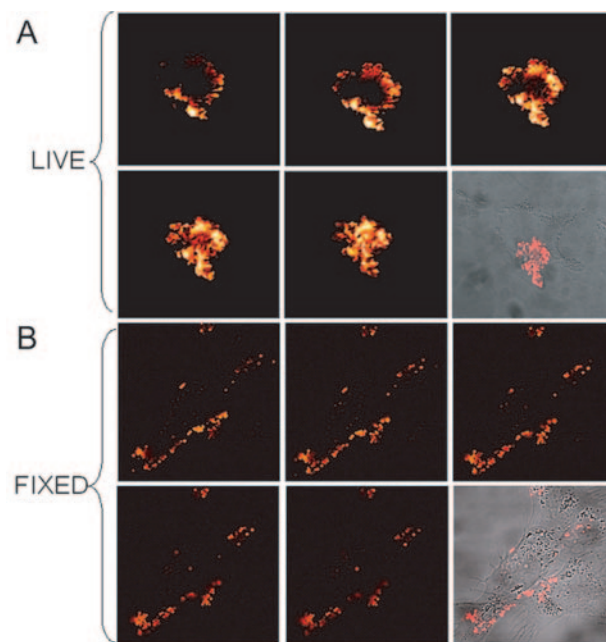


FIG. 4. Results of confocal imaging of representative cells showing the structure of cytoplasmic inclusion bodies formed from aggregates of viral genomic RNA in both a live cell (A) and fixed cells (B). Starting from the top left corner of panels A and B, each image represents a slice of the cell with a thickness of 0.5  $\mu\text{m}$ . The images were taken starting from the bottom of the cell with a 0.5- $\mu\text{m}$  gap in between (not all images are shown). The last images in both panels A and B show an overlay of the fluorescence and white-light images of the cell. Live-cell images show large, connected, amorphous inclusion bodies, while the images of inclusion bodies in fixed cell are less connected and spherical shaped.

**Confirmation of detection specificity and inclusion body composition.** To confirm that the inclusion bodies observed fluorescently as shown in Fig. 1, 3, and 4 contained viral RNA, the RNA-specific dye, SytoRNaselect (Molecular Probes) was used to stain all the RNA molecules in live cells. The results of RNA labeling of bovine turbinate cells imaged at 100 $\times$  magnification are shown in Fig. 5A and B, respectively, for infected and uninfected cells. It is clear that the inclusion bodies formed in the infected cells (shown in Fig. 5A as bright spots) could be readily observed by using the RNA-specific dye, while no inclusion bodies could be seen in the uninfected cells (Fig. 5B), which gave a diffuse fluorescent background (with three- to four-times-lower intensity) from the cytoplasmic RNA. The structure of the inclusion bodies observed in the infected cells with nonspecific RNA labeling was similar to that visualized using MBs. Note that the images shown in Fig. 5A and 5B were taken at different vertical locations of the cell and the characteristic green background is a result of live-cell autofluorescence, due to excitation with blue light.

To further confirm the specificity of the MB-based approach, we performed simultaneous staining of viral RNA and a viral protein. Specifically, live uninfected cells and cells 7 days postinfection were stained with the bRSV-specific MB; the live cells were then fixed and stained with an Alexa 488-labeled MAb for the bRSV F protein (kindly provided by C. Kelling at the University of Nebraska). This MAb (8G12) has been

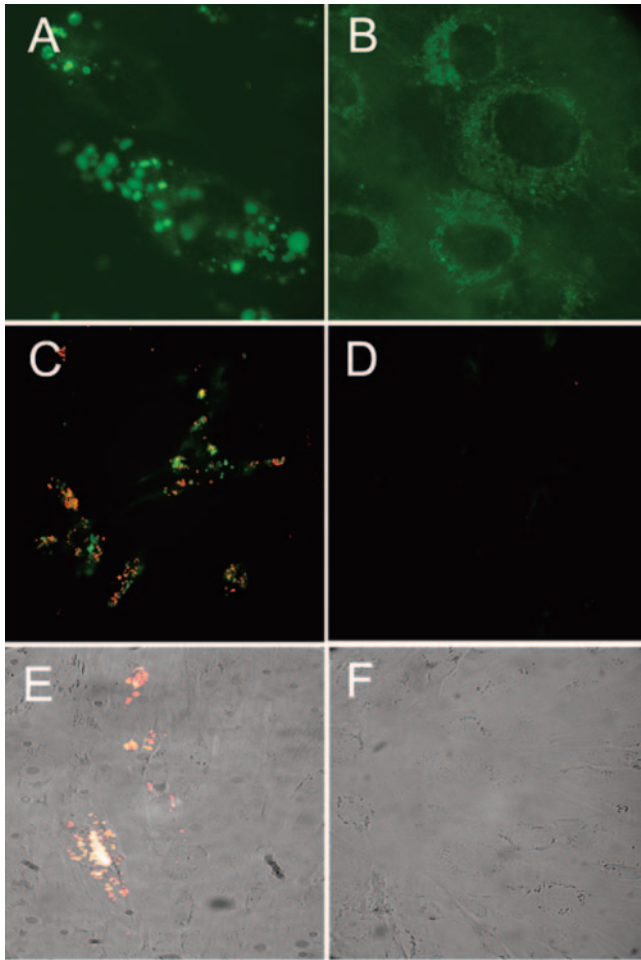


FIG. 5. Additional control studies to confirm the composition of inclusion bodies and the specificity of the MB-based method. Staining of all RNA molecules in infected (A) and uninfected (B) living cells with RNA-specific dye SytoRNaselect clearly indicated that the inclusion bodies seen in panel A only are composed predominately of RNA. Further, simultaneous MB and MAb staining of the bRSV genome and the F protein, respectively, exhibited both red (MB) and green (MAb) signals in the infected cells (C) but not in uninfected cells (D), demonstrating the high specificity of the MB-based approach in virus detection. In addition, in cells 5 days postinfection, MBs targeting bRSV showed a strong fluorescence signal (E), whereas the negative-control MB with mismatches gave a very low signal (F), further confirming the high specificity of the MB-based approach.

shown to be highly specific to the bRSV F protein (21) and is capable of staining both the envelope and cytoplasmic forms of the F protein. Figures 5C and 5D show, respectively, the fluorescence images of the infected and uninfected cells after MB staining of the viral RNA and MAb staining of the F protein. We found that only the infected cells exhibited red and green signals corresponding to MB and MAb staining, respectively (Fig. 5C), where uninfected cells gave very low background signals (Fig. 5D). This clearly demonstrates that viral detection using MBs has very high specificity. To further confirm the specificity of the MB designed to target bRSV, we compared the fluorescence signal from the bRSV-targeting MB and the mutant control MB (see Materials and Methods) in infected cells on day 5 postinfection. The MBs targeting the bRSV

genome showed very bright inclusion bodies in infected cells (Fig. 5E), whereas cells with the mutant control MB exhibited no visible fluorescence (Fig. 5F), thereby demonstrating the high specificity of the bRSV targeting MB.

In summary, in this study we were able to characterize a clinical isolate of bRSV rapidly and quantitatively while the cells were still alive and the virus was active. Using molecular beacons combined with efficient delivery and fluorescence microscopy, many aspects of viral pathogenesis, from subcellular organization to cell-to-cell spreading, can be studied in real time with single-cell and even single-molecule detail. For the first time, the imaging of the structure of cytoplasmic inclusion bodies (viral RNA aggregates) was demonstrated with live cells and an active virus. In addition, using molecular imaging in conjunction with a viral growth model, viral spreading could be analyzed quantitatively. Future studies will combine molecular beacon-based RNA detection with fluorescent-protein-based protein targeting to gain insight into how viral RNA and proteins interact, allowing for the study of inclusion body formation and the mechanisms that contribute to virulence in highly pathogenic viruses. It is also important to consider other virus-cell systems such as influenza virus and human immunodeficiency virus and compare the MB-based approach with existing diagnostic tools.

#### ACKNOWLEDGMENTS

This work was supported in part by NSF (BES-0222211) and NIH (1 P20 GM072069-01).

#### REFERENCES

1. Abravaya, K., J. Huff, R. Marshall, B. Merchant, C. Mullen, G. Schneider, and J. Robinson. 2003. Molecular beacons as diagnostic tools: technology and applications. *Clin. Chem. Lab. Med.* **41**:468–474.
2. Bitko, V., A. Musiyenko, O. Shulyayeva, and S. Barik. 2005. Inhibition of respiratory viruses by nasally administered siRNA. *Nat. Med.* **11**:50–55.
3. Bonhoeffer, S., R. M. May, G. M. Shaw, and M. A. Nowak. 1997. Virus dynamics and drug therapy. *Proc. Natl. Acad. Sci. USA* **94**:6971–6976.
4. Bratu, D. P., B. J. Cha, M. M. Mhlanga, F. R. Kramer, and S. Tyagi. 2003. Visualizing the distribution and transport of mRNAs in living cells. *Proc. Natl. Acad. Sci. USA* **100**:13308–13313.
5. Brodsky, A. S., and P. A. Silver. 2002. Identifying proteins that affect mRNA localization in living cells. *Methods* **26**:151–155.
6. Cianci, C., D. R. Langley, D. D. Dischino, Y. Sun, K. L. Yu, A. Stanley, J. Roach, Z. Li, R. Dalterio, R. Colonno, N. A. Meanwell, and M. Krystal. 2004. Targeting a binding pocket within the trimer-of-hairpins: small-molecule inhibition of viral fusion. *Proc. Natl. Acad. Sci. USA* **101**:15046–15051.
7. Collins, P. L., L. E. Dickens, A. Buckler-White, R. A. Olmsted, M. K. Spriggs, E. Camargo, and K. V. Coelingh. 1986. Nucleotide sequences for the gene junctions of human respiratory syncytial virus reveal distinctive features of intergenic structure and gene order. *Proc. Natl. Acad. Sci. USA* **83**:4594–4598.
8. Easton, A. J., J. B. Domachowski, and H. F. Rosenberg. 2004. Animal pneumoviruses: molecular genetics and pathogenesis. *Clin. Microbiol. Rev.* **17**:390–412.
9. Faria, M., D. G. Spiller, C. Dubertret, J. S. Nelson, M. R. White, D. Scherman, C. Helene, and C. Giovannangeli. 2001. Phosphoramidate oligonucleotides as potent antisense molecules in cells and in vivo. *Nat. Biotechnol.* **19**:40–44.
10. Fearn, R., M. E. Peeples, and P. L. Collins. 2002. Mapping the transcription and replication promoters of respiratory syncytial virus. *J. Virol.* **76**:1663–1672.
11. Forrest, K. M., and E. R. Gavis. 2003. Live imaging of endogenous RNA reveals a diffusion and entrapment mechanism for nanos mRNA localization in *Drosophila*. *Curr. Biol.* **13**:1159–1168.
12. Fung, Y. W., L. T. Lau, and A. C. Yu. 2004. The necessity of molecular diagnostics for avian flu. *Nat. Biotechnol.* **22**:267.
13. Fusco, D., N. Accornero, B. Lavoie, S. M. Shenoy, J. M. Blanchard, R. H. Singer, and E. Bertrand. 2003. Single mRNA molecules demonstrate probabilistic movement in living mammalian cells. *Curr. Biol.* **13**:161–167.
14. Garcia, J., B. Garcia-Barreno, A. Vivo, and J. A. Melero. 1993. Cytoplasmic inclusions of respiratory syncytial virus-infected cells: formation of inclusion

- bodies in transfected cells that coexpress the nucleoprotein, the phosphoprotein, and the 22K protein. *Virology* **195**:243–247.
15. **Glotzer, J. B., R. Saffrich, M. Glotzer, and A. Ephrussi.** 1997. Cytoplasmic flows localize injected oskar RNA in *Drosophila* oocytes. *Curr. Biol.* **7**:326–337.
  16. **Henrickson, K. J.** 2004. Advances in the laboratory diagnosis of viral respiratory disease. *Pediatr. Infect. Dis. J.* **23**(Suppl. 1):S6–S10.
  17. **Henrickson, K. J., S. Hoover, K. S. Kehl, and W. Hua.** 2004. National disease burden of respiratory viruses detected in children by polymerase chain reaction. *Pediatr. Infect. Dis. J.* **23**(Suppl. 1):S11–S18.
  18. **Huang, Q., and T. Pederson.** 1999. A human U2 RNA mutant stalled in 3' end processing is impaired in nuclear import. *Nucleic Acids Res.* **27**:1025–1031.
  19. **Jacobson, M. R., and T. Pederson.** 1998. Localization of signal recognition particle RNA in the nucleolus of mammalian cells. *Proc. Natl. Acad. Sci. USA* **95**:7981–7986.
  20. **Jairath, S., P. B. Vargas, H. A. Hamlin, A. K. Field, and R. E. Kilkuskie.** 1997. Inhibition of respiratory syncytial virus replication by antisense oligodeoxyribonucleotides. *Antiviral Res.* **33**:201–213.
  21. **Klucas, C. A., and G. A. Anderson.** 1988. Bovine respiratory syncytial virus-specific monoclonal antibodies. *Vet. Immunol. Immunopathol.* **18**:307–315.
  22. **Knipe, D. M., P. M. Howley, D. E. Griffin, R. A. Lamb, M. A. Martin, B. Roizman, and S. E. Straus (ed.).** 2001. *Fundamental virology*, 4th ed. Lippincott Williams and Wilkins, Philadelphia, Pa.
  23. **Lerch, R. A., K. Anderson, V. L. Amann, and G. W. Wertz.** 1991. Nucleotide sequence analysis of the bovine respiratory syncytial virus fusion protein mRNA and expression from a recombinant vaccinia virus. *Virology* **181**:118–131.
  24. **Levsky, J. M., S. M. Shenoy, R. C. Pezo, and R. H. Singer.** 2002. Single-cell gene expression profiling. *Science* **297**:836–840.
  25. **Levsky, J. M., and R. H. Singer.** 2003. Fluorescence in situ hybridization: past, present and future. *J. Cell Sci.* **116**:2833–2838.
  26. **Mahy, B. W., and H. Kangro.** 1996. *Virology methods manual*. Academic Press, London, United Kingdom.
  27. **Mallipeddi, S. K., and S. K. Samal.** 1992. Sequence comparison between the phosphoprotein mRNAs of human and bovine respiratory syncytial viruses identifies a divergent domain in the predicted protein. *J. Gen. Virol.* **73**:2441–2444.
  28. **Mhlanga, M. M., D. Y. Vargas, C. W. Fung, F. R. Kramer, and S. Tyagi.** 2005. tRNA-linked molecular beacons for imaging mRNAs in the cytoplasm of living cells. *Nucleic Acids Res.* **33**:1902–1912.
  29. **Molenaar, C., S. A. Marras, J. C. Slats, J. C. Truffert, M. Lemaitre, A. K. Raap, R. W. Dirks, and H. J. Tanke.** 2001. Linear 2' O-methyl RNA probes for the visualization of RNA in living cells. *Nucleic Acids Res.* **29**:E89–E99.
  30. **Nitin, N., P. J. Santangelo, G. Kim, S. Nie, and G. Bao.** 2004. Peptide-linked molecular beacons for efficient delivery and rapid mRNA detection in living cells. *Nucleic Acids Res.* **32**:e58.
  31. **Norrby, E., H. Marusyk, and C. Orvell.** 1970. Morphogenesis of respiratory syncytial virus in a green monkey kidney cell line (Vero). *J. Virol.* **6**:237–242.
  32. **Perlette, J., and W. Tan.** 2001. Real-time monitoring of intracellular mRNA hybridization inside single living cells. *Anal. Chem.* **73**:5544–5550.
  33. **Player, M. R., D. L. Barnard, and P. F. Torrence.** 1998. Potent inhibition of respiratory syncytial virus replication using a 2-5A-antisense chimera targeted to signals within the virus genomic RNA. *Proc. Natl. Acad. Sci. USA* **95**:8874–8879.
  34. **Santangelo, P. J., B. Nix, A. Tsourkas, and G. Bao.** 2004. Dual FRET molecular beacons for mRNA detection in living cells. *Nucleic Acids Res.* **32**:e57.
  35. **Shav-Tal, Y., X. Darzacq, S. M. Shenoy, D. Fusco, S. M. Janicki, D. L. Spector, and R. H. Singer.** 2004. Dynamics of single mRNPs in nuclei of living cells. *Science* **304**:1797–1800.
  36. **Sokol, D. L., X. Zhang, P. Lu, and A. M. Gewirtz.** 1998. Real time detection of DNA. RNA hybridization in living cells. *Proc. Natl. Acad. Sci. USA* **95**:11538–11543.
  37. **Spriggs, M. K., and P. L. Collins.** 1986. Human parainfluenza virus type 3: messenger RNAs, polypeptide coding assignments, intergenic sequences, and genetic map. *J. Virol.* **59**:646–654.
  38. **Tyagi, S., and O. Alsmadi.** 2004. Imaging native beta-actin mRNA in motile fibroblasts. *Biophys. J.* **87**:4153–4162.
  39. **Woolums, A. R., M. L. Anderson, R. A. Gunther, E. S. Schelegle, D. R. LaRoche, R. S. Singer, G. A. Boyle, K. E. Friebertshauser, and L. J. Gershwin.** 1999. Evaluation of severe disease induced by aerosol inoculation of calves with bovine respiratory syncytial virus. *Am. J. Vet. Res.* **60**:473–480.
  40. **Xu, Z., M. Kuang, J. R. Okicki, H. Cramer, and N. Chaudhary.** 2004. Potent inhibition of respiratory syncytial virus by combination treatment with 2-5A antisense and ribavirin. *Antiviral Res.* **61**:195–206.
  41. **Zhang, W., H. Yang, X. Kong, S. Mohapatra, H. S. Juan-Vergara, G. Hellermann, S. Behera, R. Singam, R. F. Lockey, and S. S. Mohapatra.** 2005. Inhibition of respiratory syncytial virus infection with intranasal siRNA nanoparticles targeting the viral NS1 gene. *Nat. Med.* **11**:56–62.